Multiscale white matter fiber tract coregistration: a new feature-based approach to align diffusion tensor data

A. Leemans[1], J. Sijbers[1], S. De Backer[1], E. Vandervliet[2], P. Parizel[2]

[1]Physics, University of Antwerp, Antwerp, Belgium, [2]Radiology, University Hospital Antwerp, Antwerp, Belgium

Introduction and Purpose

Diffusion tensor magnetic resonance imaging (DTI) has demonstrated to be an important diagnostic tool for various neuropathological diseases and already shows very promising results to quantitatively study the brain structure-function relationship or to investigate the brain neurodevelopment [1-4]. Here, image coregistration is indispensable to objectively quantify specific properties of multiple data sets or to perform a voxel based statistical analysis. Current coregistration methods are mainly voxel-based and therefore require the use of computationally expensive similarity measures, which is unavoidable due to the complex multi-valued nature of the diffusion tensor images, or make use of a *k*-channel scalar approach to align the DTI data sets [5-7]. Also, most of these voxel based approaches are iteratively calculating the spatial transformation and therefore may suffer from local optima. In this work, we developed an automatic multiscale three-dimensional (3D) feature-based DTI coregistration technique based on the local curvature κ and torsion τ of the White Matter (WM) fiber pathways. This fully automatic and analytic (no iterations) technique inherently allows region of interest (ROI) coregistration, is adequate to perform both global and local transformations, and makes the calculation of the diffusion tensor reorientation superfluous. Simulations with synthetic diffusion tensor data have been elaborated to evaluate the performance and an in-vivo example has been worked out, demonstrating feasibility of the proposed technique to align experimental data.

Theory

Consider two tractography data sets that need to be coregistered, i.e. the source tracts $\{\boldsymbol{\alpha}\} \equiv \{\boldsymbol{\alpha}_j \mid j = 1,\ldots,J_{\boldsymbol{\alpha}}\}$ and the target tracts $\{\boldsymbol{\beta}\} \equiv \{\boldsymbol{\beta}_j \mid j = 1,\ldots,J_{\boldsymbol{\beta}}\}$. Each tract can be parameterized by their local curvature κ and torsion τ as follows: $\boldsymbol{\alpha}_j \equiv \{\boldsymbol{\alpha}_j(\mathrm{i}) : i = 1,\ldots,N_j \rightarrow \boldsymbol{g}_i(\boldsymbol{\alpha}_j) \equiv (\kappa_i, \tau_i)\}$ and $\boldsymbol{\beta}_j \equiv \{\boldsymbol{\beta}_j(\mathrm{i}) : i = 1,\ldots,M_j \rightarrow \boldsymbol{g}_i(\boldsymbol{\beta}_j) \equiv (\kappa_i, \tau_i)\}$, where N_j and M_j represent the number of sample points of the tract space curves $\boldsymbol{\alpha}_j$ and $\boldsymbol{\beta}_j$, respectively. Any subcurve of $\boldsymbol{\alpha}_j$ and $\boldsymbol{\beta}_j$ containing K consecutive points is denoted as $\boldsymbol{\alpha}_{Kj}$ and $\boldsymbol{\beta}_{Kj}$, respectively. For every source subcurve, the corresponding target subcurve can now determined by minimizing the Mean Squared Difference (MSD) between different tract curves as follows: $\forall\, j \in \{1,\ldots,J_{\boldsymbol{\alpha}}\}, \exists\, k \in \{1,\ldots,J_{\boldsymbol{\beta}}\} : (\boldsymbol{\alpha}_{Kj}, \boldsymbol{\beta}_{Kj}) = \arg\min_{\{m,L\}} \mathrm{MSD}(\boldsymbol{\alpha}_{Lj}, \boldsymbol{\beta}_{Lm})$ with $\mathrm{MSD}(\boldsymbol{\alpha}_{Lj}, \boldsymbol{\beta}_{Lm}) \equiv L^{-1}\sum_i \| \boldsymbol{g}_i(\boldsymbol{\alpha}_{Lj}) - \boldsymbol{g}_i(\boldsymbol{\beta}_{Lm}) \|^2$ and $L \in \{L_{\min}, \ldots, \min(N_j, M_j)\}$, where $L_{\min}$ is a predefined parameter, denoting the minimum number of sample points that represent a subcurve. For each set of corresponding curves $(\boldsymbol{\alpha}_{Kj}, \boldsymbol{\beta}_{Kj})$, principal component analysis is applied to find the local transformation $\boldsymbol{\Phi}_j$ that maps $\boldsymbol{\alpha}_{Kj}$ to $\boldsymbol{\beta}_{Kj}$. Finally, the optimal transformation $\boldsymbol{\Omega}$ is calculated from $\{\boldsymbol{\Phi}_j\}$. To make the coregistration more robust, an evolution based multiscale method is incorporated. In this approach, a tract curve $\boldsymbol{\alpha}$ is convolved with a Gaussian kernel G_σ with mean 0 and standard deviation $\sigma = 1,\ldots,S$ for computing the varying levels of detail, i.e. $\boldsymbol{\alpha}_\sigma = \boldsymbol{\alpha} * G_\sigma$. The resulting final transformation can now be found as follows: $\boldsymbol{\Psi} = \arg\min_{\boldsymbol{\Omega}} \mathrm{MSD}[\{\boldsymbol{\beta}\}, \{\boldsymbol{\gamma}\} \equiv \boldsymbol{\Omega}(\{\boldsymbol{\alpha}_\sigma\})]$, where $\{\boldsymbol{\gamma}\}$ represent the coregistered tract curves. To increase the coregistration precision, only the p percent best local transformations $\boldsymbol{\Phi}_j$ are included in the estimation of $\boldsymbol{\Omega}$. Also, a tract curve sampling factor ξ is defined that uniformly samples the tracts to reduce the computational complexity.

Methods

First, the coregistration performance is evaluated by means of a simulated DT-MRI phantom [8]. Next, the coregistration technique is tested on experimental data. Two in vivo DTI data sets of the (healthy) human brain (male, 25y) were acquired on a 1.5 Tesla MR system. Thereby, 60 axial slices with thickness of 2 mm were obtained covering the whole brain (voxel size of 2×2×2 mm^3). A gradient configuration with 60 directions was used and additional acquisition parameters were as follows: *b*-factor = 700 s/mm^2, RT = 8.3 s, ET = 108 ms, and number of b_0 (no diffusion weighting) averages = 10.

Results

Simulated DTI phantom: Fig. 1 (a) and (b) represent the tractography results of, respectively, a noiseless target (ground truth rotation is $\theta_z = 30°$) and a noisy source synthetic DTI phantom (with $J_{\boldsymbol{\alpha}} \approx J_{\boldsymbol{\beta}} \approx 10^3$). The ellipsoids depict the local diffusion properties and the background gray scaling reflects the corresponding fractional anisotropy value. In Fig. 2, the effect of noise on the coregistration accuracy is shown for a large number of trials (10, 10^2, and 10^3). Fig. 3 demonstrates the benefit of the applied multiscale approach: in (a) the (normalized) global coregistration residue ε and (b) the corresponding θ_z are shown as function of the level of detail σ. Finally, Fig. 4 and Fig. 5 elucidate the effect of the user-defined parameters p and ξ, respectively, on the coregistration result.

Experimental DTI data: Fig. 6 shows the tractography results of the experimental DTI data sets, i.e. the target tracts $\{\boldsymbol{\beta}\}$ (red) and the source tracts $\{\boldsymbol{\alpha}\}$ (green) (with $J_{\boldsymbol{\alpha}} \approx J_{\boldsymbol{\beta}} \approx 10^4$; p = 10%; $\xi = 5$; $\sigma = 0 \rightarrow 20$). Note that despite the difference in field of view (FOV), as indicated in orange, the coregistered tracts are still correctly aligned with the target tracts, demonstrating the feasibility of ROI coregistration.

Discussion and conclusions

In this work, we developed a non-iterative multiscale 3D-rigid-body coregistration technique for WM fiber tractography data. Simulations have been performed demonstrating a high coregistration accuracy and precision as a function of different noise levels and several user-defined parameters. The method has been tested on experimental data and has shown to be robust under non-trivial experimental conditions.

References

[1] Basser P et al., *Biophys J* **66**, p. 259-267, 1994; [2] Mori S et al., *NMR biomed* **15**, p. 468-480, 2002; [3] Snook L et al., *NeuroImage* **26**, p. 1164-1173, 2005. [4] Salat DH et al., *Neurobiology of Aging* **26**, p. 1215-1227, 2005; [5] Jones D et al., *NeuroImage* **17**, p. 592-617, 2002; [6] Alexander DC et al., *IEEE Trans Med Imag* **20**, p. 1131-1139, 2001; [7] Park HJ et al., *NeuroImage* **20**, p. 1995-2009, 2003. [8] Leemans A et al., *Magn Reson Med* **53**, p. 944-953, 2005.

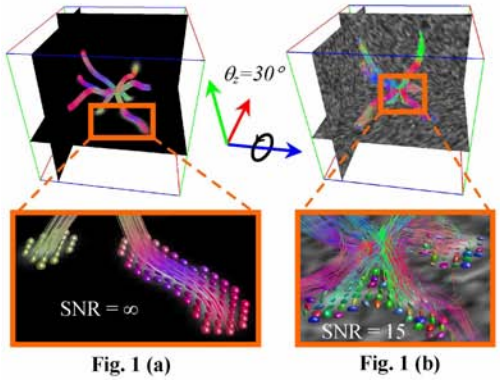

Fig. 1 (a) Fig. 1 (b)

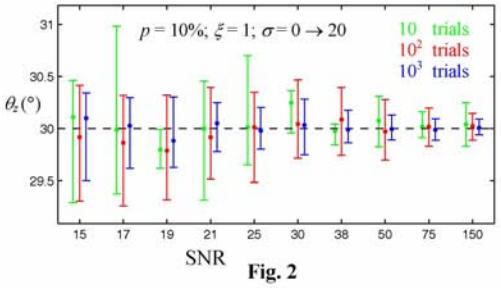

Fig. 2

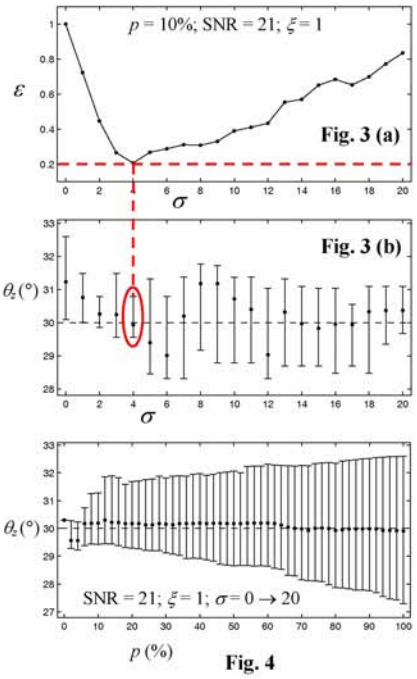

Fig. 4

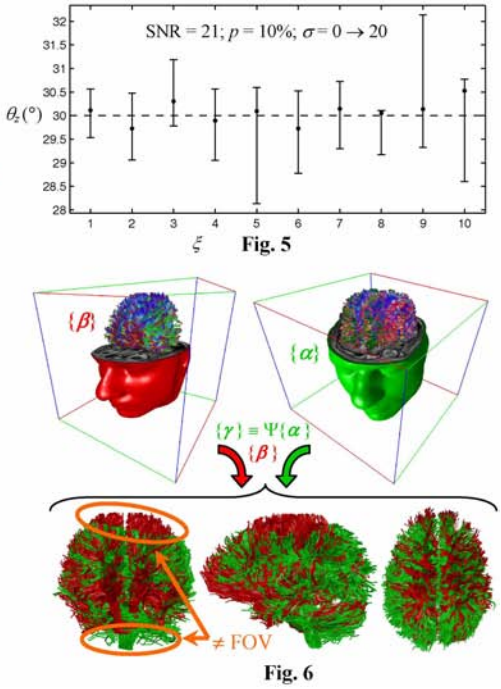

Fig. 5

Fig. 6